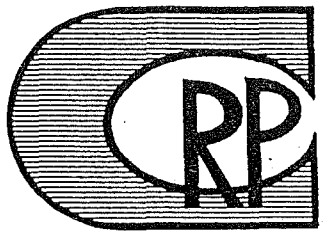

文部省科学研究費補助金重点領域研究

反応性プラズマの制御

領域番号032　　研究成果報告書

Report

on

CONTROL OF REACTIVE PLASMAS

1988-1991 FY

edited by
R. Itatani
Department of Electronics
Faculty of Engineering
Kyoto University

supported by
Grant-in-Aid for Scientific Research
on Priority Areas
Ministry of Education, Science and Culture

March 1992

MEASUREMENT OF NON-EMISSIVE RADICALS IN REACTIVE PLASMAS USING SPECTROSCOPIC TECHNIQUES
分光法による反応性プラズマ内の非発光ラジカル密度計測

Toshio GOTO, Akihiro KONO and Shigeru KISHIMOTO
Department of Information Electronics,
Nagoya University, Nagoya 464-01
後藤俊夫、河野明広、岸本　茂
名古屋大学工学部電子情報学科
〒464-01　名古屋市千種区不老町
Mineo HIRAMATSU
Department of Electrical and Electronic Engineering,
Meijo University, Nagoya 468
平松美根男
名城大学理工学部電気電子工学科
〒468 名古屋市天白区天白町
Eizi HIROTA
The Graduate University for Advanced Studies,
Yokohama 227
廣田榮治
総合研究大学院大学
〒227 横浜市緑区長津田町
Chikashi YAMADA
Optoelectronics Technology Research Corporation,
Tsukuba 300-26
山田千樫
光技術研究開発（株）
〒300-26　つくば市東光台

Abstract

We have established a method for measuring radical densities in reactive plasmas using infrared diode laser absorption spectroscopy (IRLAS). The technique was used to investigate the density, rotational temperature, reaction rate constant and diffusion coefficient of radicals (SiH, SiH_3, CF, and CF_3) in silane and fluorocarbon plasmas; a high-resolution infrared spectrum of the SiH_2 radical was also studied by using IRLAS. Ultraviolet absorption spectroscopic studies were carried out to measure the Si atomic radical density in silane plasmas. Further, a new method of determining radiative transition probabilities by use of a laser induced fluorescence technique was developed.

1 Introduction

Neutral radicals play an important role in thin film deposition or etching of materials by using reactive plasmas. In order to understand the fundamental mechanisms of such plasma processing, it is indispensable to obtain information about neutral radicals. The majority of the radicals in reactive plasmas usually exist in their ground states and thus they are non-emissive. Therefore, quantitative measurements of neutral radical densities were rather difficult and very few studies have been reported.

The purpose of this research has been to develop methods for quantitative measurements of various radical densities using spectroscopic techniques and actually to measure radical densities in reactive plasmas;

spectroscopic techniques allow us to detect radicals without perturbing plasmas. The results of this research (carried out by two research units) are summarized in this report as follows. In Sec. 2, we describe the development of an infrared diode laser absorption spectroscopic (IRLAS) technique for measuring radical densities and their application to the measurements of SiH_3 and SiH radical densities in silane plasmas. Section 3 describes the measurements of Si atomic radical densities in silane plasmas by using ultraviolet absorption spectroscopic techniques. IRLAS was used to obtain a high resolution spectrum of the SiH_2 radical, from which accurate molecular constants were determined; the results are shown in Sec. 4. IRLAS measurements were also carried out for radical densities in fluorocarbon plasmas, the results being summarized in Sec. 5. For quantitative spectroscopic measurements, the knowledge of Einstein A coefficient is essential. We have developed a new method to determine Einstein A coefficient by using a laser induced fluorescence (LIF) technique; the results are described in Sec. 6.

2 Measurements of Radical Densities in Silane Plasmas Using Infrared Diode Laser Absorption Spectroscopy

Plasma CVD processes using a silane gas are used to produce hydrogenated amorphous silicon (a-Si:H) thin films, which are widely employed in useful electronic devices such as solar cells and thin-film transistor arrays. Among various species in silane plasmas, neutral radicals in the ground electronic states, in particular SiH_3, are regarded as the dominant precursors of the film. In order to measure radical densities in silane plasmas, we have developed a method based on infrared diode laser absorption spectroscopy (IRLAS). The method was first applied to the measurement of the SiH_3 and SiH radicals in a pulsed DC discharge. Then it was applied to the measurement of the SiH_3 radical in an RF discharge similar to those used commonly for actual film deposition. The correlation of the SiH_3 density with the film deposition rate was investigated. In addition, some reaction rate constants and diffusion coefficients of the radicals were determined.

2.1 SiH_3 density in DC pulsed SiH_4/H_2 discharge

IRLAS system and principle of measurements

Figure 2.1 shows the schematic block diagram of the infrared diode laser absorption spectrometer. The diode laser is cooled down to 10-80 K using a helium compresser. Its frequency is coarsely adjusted by varying the temperature and then is scanned by changing the current. The laser linewidth is much narrower than the widths of absorption lines to be measured. In addition to the main absorption cell, the laser beam is provided for a reference gas cell and a 25-cm confocal etalon. The reference gas (acetylene was used in the SiH_3 measurements) gives the absorption signal used as an absolute wavenumber marker, while the etalon produces a fringe pattern (0.01-cm^{-1} spacing) used as a relative wavenumber marker. The laser current is slightly modulated at f=5 kHz for the lock-in detection of the reference spectrum and the interference fringes. The main absorption signal from the laser beam passing through the discharge plasma is recorded by a transient memory. The SiH_3 absorption spectrum is obtained by taking the difference between the signals accumulated for two gate periods, one after and the other before the start of the pulsed discharge, while the laser frequency is scanned

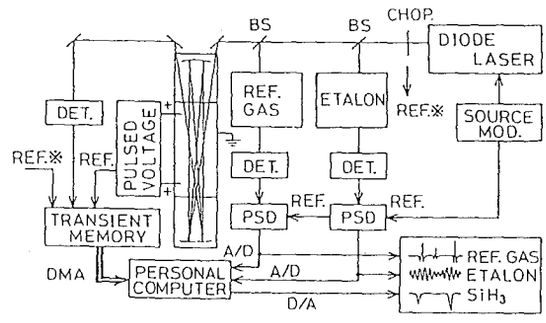

Fig. 2.1. Schematic block diagram of the infrared diode laser spectrometer

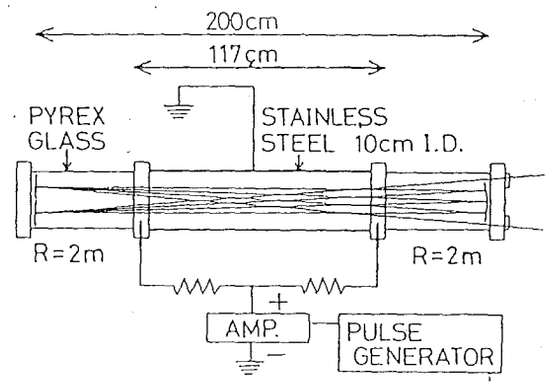

Fig. 2.2. Discharge tube and White-type multireflection system

slowly.

Figure 2.2 shows the discharge tube and the White-type multireflection system used in this study. The discharge tube consists of a stainless-steel cylindrical hollow cathode (10-cm diameter and 117-cm long) and two tungsten pin anodes. A pulsed DC voltage is applied between the electrodes. The infrared laser beam is adjusted to pass 40 times through the discharge tube so that the total absorption pass length is 4680 cm.

The radical density N in the lower level of the absorption line can be calculated using the formula:[1)]

$$N = (8\pi c\nu^2)(g_L/g_U A)\int k(\nu)d\nu\ , \qquad (2.1)$$

where g_U and g_L are, respectively, the statistical weights of the upper and lower level of the absorption line, c the speed of light, ν the wavenumber, A the Einstein A coefficient, and $k(\nu)$ the absorption coefficient given by

$$k(\nu)=-(1/L)\times \ln[\{I_0(\nu)-I_a(\nu)\}/I_0(\nu)]. \qquad (2.2)$$

Here, L is the absorption length, $I_0(\nu)$ the laser intensity without absorption, and $I_a(\nu)$ the absorption intensity. In Eq. (2.1), it is assumed that the radical density in the upper level is negligible. The absorption coefficient $k(\nu)$ in Eq. (2.1) was integrated over a Gaussian profile corresponding to a certain translational temperature which was assumed to be equal to the rotational temperature.

Rotational temperature and SiH_3 density

A SiH_4/H_2 mixture (SiH_4/H_2=0.065/0.585 Torr) was introduced into the discharge tube at the total flow rate of 60 sccm and excited by a pulsed discharge with a duration time of 0.45 ms, repetition frequency of 9 Hz, and peak current of 1 A. Absorption measurements were carried out for a number of Q-branch lines in the $\nu_2(1\leftarrow 0)$ band of the ground electronic state (X^2A_1) of SiH_3. An example of the observed absorption line profile is shown in Fig. 2.3. The radical densities in the lower level of the absorption lines were calculated by using an Einstein A coefficient based on an *ab-initio* MO calculation.[2)] Figure 2.4 shows the obtained radical density (per unit statistical weight) plotted in semi-log scale as a function of the rotational term value. All the data points are closely located on a straight line, indicating that the SiH_3 radicals are in thermal equilibrium with respect to the population distribution over the rotational levels. The slope of the straight line gives a rotational temperature of

$$T_r = 320\pm 10\ \mathrm{K}.$$

Then, assuming that the vibrational temperature is equal to the rotational temperature, the total SiH_3 density in the ground electronic state can be calculated using the rotational and vibrational partition functions;[3] the result is

$$N(SiH_3)=(5.9\pm 0.3)\times 10^{11}\ cm^{-3}.$$

Diffusion coefficient and reaction rate constant

Figure 2.5 shows a transient absorption waveform of the SiH_3 radical. The dominant loss processes of SiH_3 in the plasma are the diffusion to the wall and the following recombination and disproportionation reactions:

$$SiH_3 + SiH_3 \rightarrow Si_2H_6 \qquad (2.3)$$
$$SiH_3 + SiH_3 \rightarrow SiH_2 + SiH_4. \qquad (2.4)$$

Thus the SiH_3 density N after the turn-off of the discharge will approximately follow the rate equation given by

$$dN/dt = -2kN^2 - N/\tau\ , \qquad (2.5)$$

where k is the sum of the rate constants of the reactions (2.3) and (2.4), and τ is the diffusion lifetime. This equation can be solved analytically and by fitting the solution to the observed decay of the density as shown in Fig. 2.5, we can estimate k and τ. For SiH_4(10%)/H_2 mixtures, the values of k thus obtained are

$$k = (1.5 \pm 0.6)\times 10^{-10}\ cm^3\cdot s^{-1};$$

and they are relatively insensitive to the total pressure in the studied range of 40-130 mTorr. The value of τ was found to be linearly proportional both to the total pressure and to the H_2 partial pressure. This means that the following Blanc's equation[4] is approximately valid:

$$\frac{P(SiH_4/H_2)}{D(SiH_3 \text{ in } SiH_4/H_2)} = \frac{P(H_2)}{D(SiH_3 \text{ in } H_2)} + \frac{P(SiH_4)}{D(SiH_3 \text{ in } SiH_4)}, \qquad (2.6)$$

where D's are diffusion constants and P's are pressures. With the aid of this equation, the following diffusion constants were derived from the pressure dependence of τ :

$$D(SiH_3 \text{ in } H_2) = 580\pm 140\ cm^2\cdot Torr\cdot s^{-1}$$
$$D(SiH_3 \text{ in } SiH_4) = 140\pm 30\ cm^2\cdot Torr\cdot s^{-1}.$$

Dependence of the SiH_3 density on the pressure

For gas mixtures of SiH_4/H_2, SiH_4/Ar, and SiH_4/He, the dependence of the SiH_3 radical density on the total pressure and on the buffer-gas partial pressure was investigated. The discharge current was 1 A and the discharge pulse width was kept at 0.45 ms. Here we mainly quote the results for the SiH_4/H_2 mixture. Figure 2.6 shows the results of measurements in which the total pressure was varied with the SiH_4 partial pressure kept at 10% of the total pressure. Figure 2.7 shows the H_2 partial pressure dependence of the radical density. Under the present experimental conditions, the dominant production process of SiH_3 is the electron impact dissociation of SiH_4, while the dominant loss process is diffusion. In Fig. 2.6 the SiH_3 density decreases in the high total pressure region and in Fig. 2.7 it decreases with increasing H_2 partial pressure. Since the diffusion loss rate decreases with increasing pressure, this behavior should be ascribed to the decrease of the SiH_3 production rate, caused presumably by the decrease of the electron temperature. We also measured the dependence of the SiH_3 radical density on the dis-

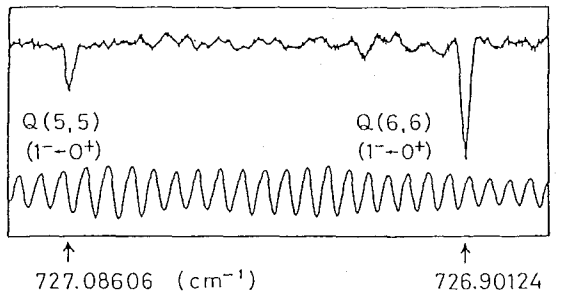

Fig. 2.3. Observed absorption profiles of SiH_3 lines. The lower trace is the fringe pattern from the etalon (0.01-cm^{-1} interval).

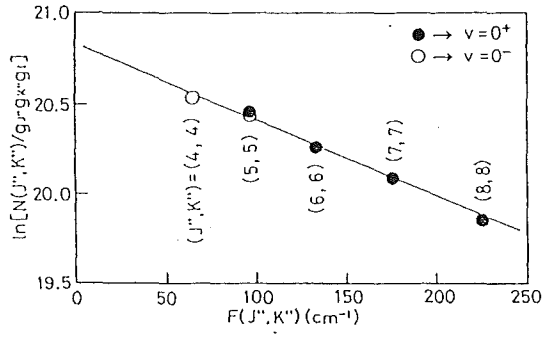

Fig. 2.4. Radical density plotted against the rotational term value. The open circles refer to $v=1^+ \leftarrow 0^-$ and the solid circles to $v=1^- \leftarrow 0^+$. The slope gives the rotational temperature of 320± 10 K.

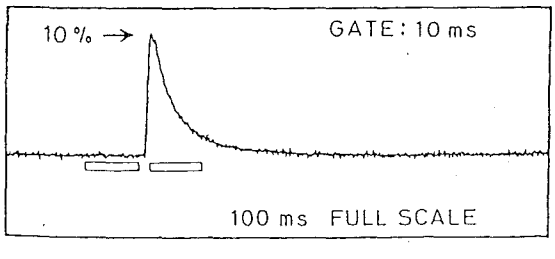

Fig. 2.5. Transient absorption waveform of the SiH_3 $Q(6,6)(1^- \leftarrow 0^+)$ line with two time gates. The pressure was SiH_4/H_2=0.085/0.765 Torr, the flow rate 60 sccm, the pulse width 0.45 ms and the discharge current 1 A.

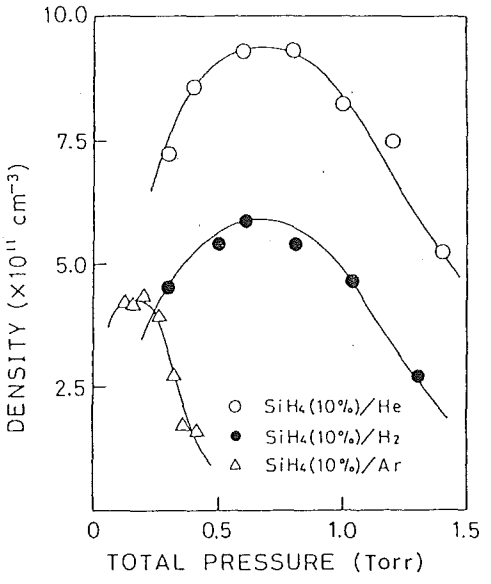

Fig. 2.6. SiH_3 density plotted against the total pressure.

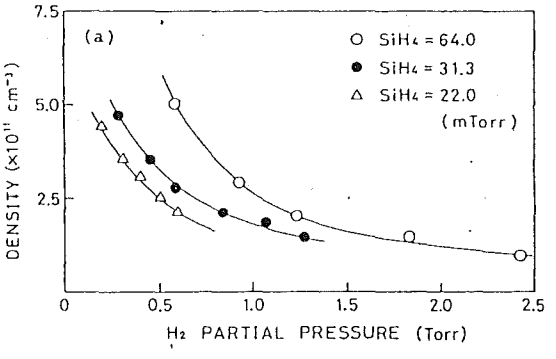

Fig. 2.7. SiH_3 density plotted against the H_2 partial pressure.

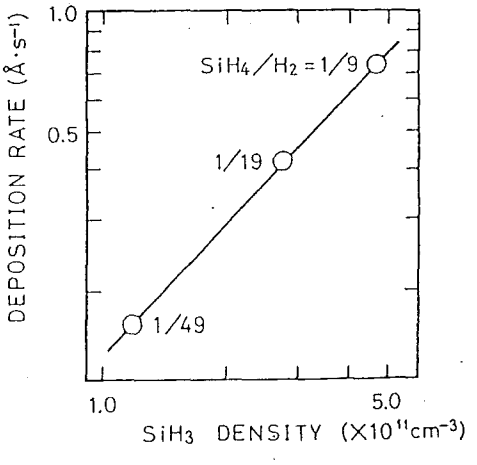

Fig. 2.8. Deposition rate of thin film plotted against the SiH_3 radical density.

charge pulse width; the results indicated that the SiH_3 density increased linearly with the pulse width in the measured pulse width range of 0-1 ms. This means that the SiH_3 density in the steady-state should be higher than those shown in Figs. 2.6 and 2.7 approximately by a factor given by the ratio between the diffusion lifetime and the discharge pulse width.

Correlation between the SiH_3 density and the a-Si:H film growth rate

The growth rate of a-Si:H film was measured at various H_2 partial pressures with the SiH_4 partial pressure fixed at 31 mTorr; the discharge pulse width was fixed at 0.45 ms and the discharge current at 1 A. The growth rate was obtained by dividing the film thickness by the deposition time. The correlation between the SiH_3 density and the film growth rate is shown in Fig. 2.8. The linear relationship between these quantities suggests that SiH_3 is responsible for film growth.

2.2 SiH density in DC pulsed SiH_4/Ar discharge

The IRLAS setup used to determine SiH radical densities was essentially the same as described in Sec. 2.1; OCS was used as a reference gas. A 680-Hz AC voltage was half-wave rectified and used to generate a SiH_4/Ar plasma. Several rovibrational lines in $X^2\Pi_{1/2}(1\leftarrow 0)$ and $X^2\Pi_{3/2}(1\leftarrow 0)$ were measured to derive the rotational temperature under the condition of the peak discharge current of 700 mA, peak voltage of 0.7 kV, SiH_4/Ar pressure of 0.17/0.35 Torr, and total flow rate of 150 sccm; the resulting rotational temperature was $(4.0\pm 0.3)\times 10^2$ K. Using this value, the total SiH radical density in the ground electronic state ($X^2\Pi$, v=0) was calculated; the Einstein A coefficient necessary for the calculation was taken from an *ab-initio* MO calculation.[2] Figures 2.9 and 2.10

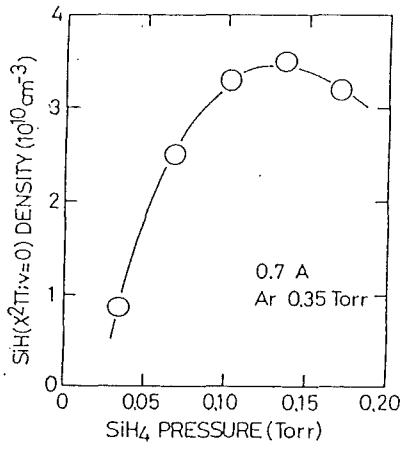

Fig. 2.9. Dependence of the peak SiH radical density on the SiH_4 partial pressure.

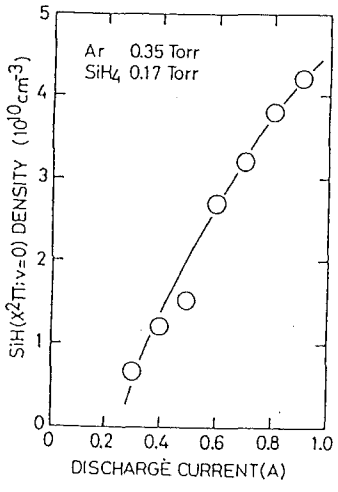

Fig. 2.10 Dependence of the peak SiH radical density on the discharge current.

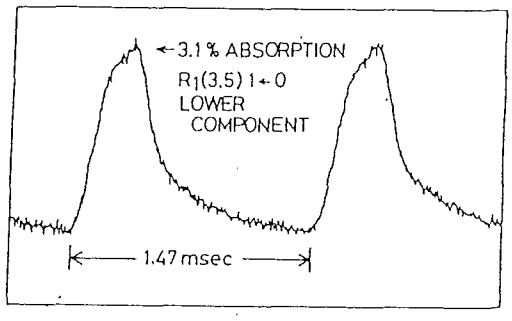

Fig. 2.11 Transient absorption waveform of SiH $R_1(3.5)$ lower component.

show the dependence of the SiH density (peak value) on the SiH_4 partial pressure and on the discharge current, respectively.

The observed transient absorption waveform of $R_1(3.5)$ lower component is shown in Fig. 2.11 The diffusion lifetime of the SiH radical under the plasma condition investigated was estimated to be about an order of magnitude longer than the SiH density decay shown in Fig. 2.11. Thus the major loss process of the SiH radical in the silane plasma should be the reaction with SiH_4:

$$SiH + SiH_4 \rightarrow \text{products}. \qquad (2.7)$$

Then, the decay time constant τ of the SiH density in Fig. 2.11 can be related to the rate constant k of the reaction (2.7) as

$$1/\tau = kN(SiH_4), \qquad (2.8)$$

where $N(SiH_4)$ is the SiH_4 density in the plasma. The decay of the SiH density in Fig. 2.11 was well fitted by a single-exponential function, giving

$$\tau = (0.28 \pm 0.03) \text{ ms}.$$

The decomposition percentage of SiH_4 in the plasma was estimated to be $(73 \pm 5)\%$ from the absorption intensity of a SiH_4 line, and therefore

$$N(SiH_4) = (1.1 \pm 0.2) \times 10^{-15} \text{ cm}^{-3}.$$

From these data the reaction rate constant k is determined to be

$$k = (3.2 \pm 0.9) \times 10^{-12} \text{ cm}^3 \cdot \text{s}^{-1}.$$

This value agrees with that measured by using LIF technique to within the limit of errors.[5)]

2.3 SiH_3 density in RF SiH_4/H_2 discharge

Experimental setup

The IRLAS system was extended to be able to measure the spatial distribution of radicals in RF discharge plasmas. The RF P-CVD chamber employed in this study is shown in Fig. 2.12. Two stainless-steel circular plates (20-cm diameter and 3-cm apart) were used as the electrodes. The IR laser beam was passed 60 times through the plasma region, and absorption path length was assumed to be 20cm× 60=1200cm, although some SiH_3 radicals may escape from the region between the electrodes. The spatial distribution of the radical density was observed by moving the chamber vertically, whereas the multireflected path of the IR laser beam was fixed in space. A modulated RF(13.56 MHz) voltage was applied to the electrodes with RF-on period 7.5 ms and RF-off period of 11.0 ms; the input power in the RF-on period was 125 W (0.40 Wcm^{-2}).

Spatial distribution of the SiH_3 density

The spatial distribution of the SiH_3 density was investigated for a SiH_4/H_2 mixture (SiH_4/H_2=50/30 mTorr). The observed transient absorption waveform indicated that the SiH_3 density reached a stationary level during the RF-on period. The rotational temperature was determined from the absorption intensities of four Q-branch lines to be

$$T_r = 410 \pm 40 \text{ K}.$$

By using this value, the total SiH_3 density in the ground electronic state was calculated. Figure 2.13 shows the obtained spatial distribution of the total SiH_3 density.

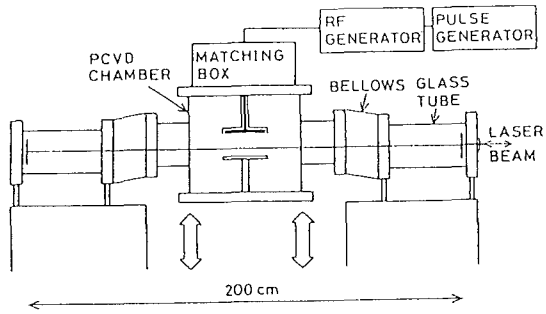

Fig. 2.12 RF silane P-CVD chamber with a White-type multiple reflection system.

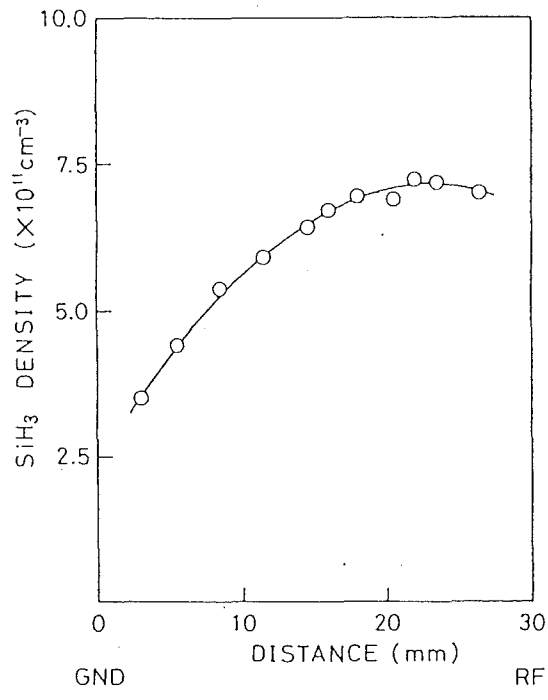

Fig. 2.13 Observed spatial distribution of the SiH_3 radical.

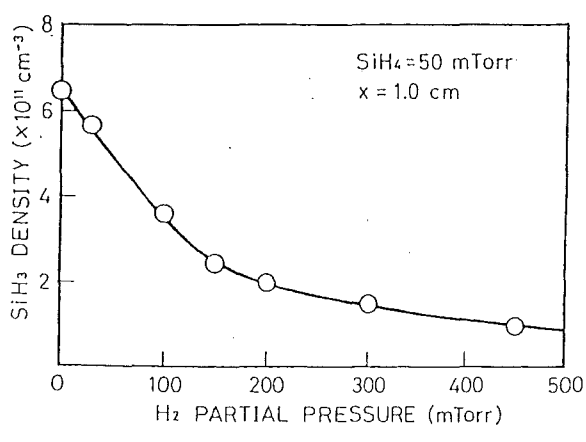

Fig. 2.14 SiH_3 radical density plotted against the H_2 partial pressure.

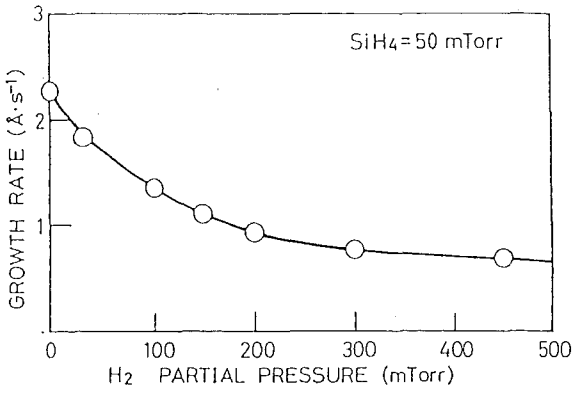

Fig. 2.15 Growth rate of the a-Si:H film plotted against the H_2 partial pressure.

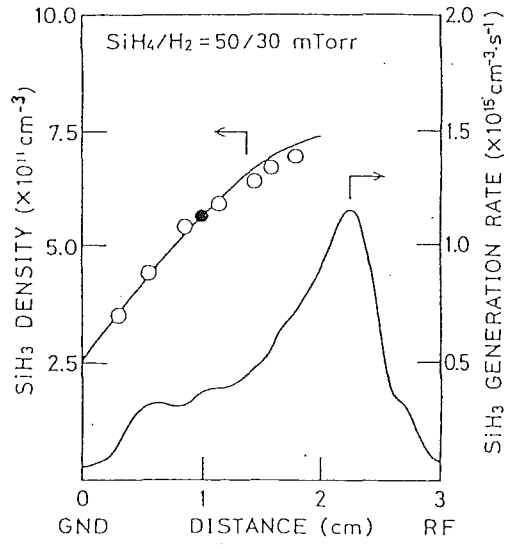

Fig. 2.16 Calculated (upper solid curve) and measured (open circles) spatial distributions of the SiH_3 density. The lower solid curve is the SiH_3 generation rate estimated from the SiH emission intensity.

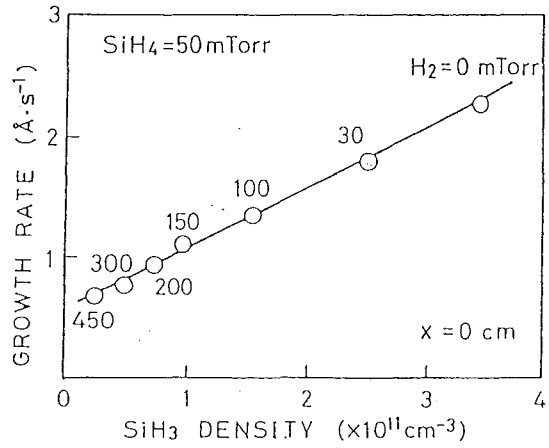

Fig. 2.17 Growth rate of the a-Si:H film plotted against the SiH_3 density at x=0 mm.

Under the same discharge condition, a quartz substrate was placed at the center of the grounded electrode, and a-Si:H film was deposited without heating the substrate. The growth rate of a-Si:H in the RF-on period was found from the film thickness to be

$$R_{meas} = 1.79\ A \cdot s^{-1},$$

assuming that deposition rate was constant during the RF-on period and zero during the RF-off period.

On the other hand, we can estimate the SiH_3 flux to the substrate from the SiH_3 density gradient near the substrate surface (Fig. 2.13); then, by using this flux, we can estimate the rate of the film growth due solely to the SiH_3 radical, with the aid of the SiH_3 sticking probability[6] and other necessary parameters.[7] The resulting value is

$$R_{SiH3} = 1.1\ A \cdot s^{-1}.$$

Though this value may suffer from the uncertainties of a number of parameters used, it certainly amounts to a significant fraction of R_{meas}, demonstrating that the SiH_3 radical is an important contributor to the a-Si:H film growth.

Correlation between the SiH_3 density and the growth rate of a-Si:H film

The SiH_3 density at 10 mm above the grounded electrode was determined as a function of the H_2 partial pressure, with the SiH_4 pressure fixed at 50 mTorr and its flow rate at 10 sccm; we assumed a rotational temperature of 410 K. The result is shown in Fig. 2.14. The growth rate (in the RF-on period) of the a-Si:H thin film was measured in the same experimental conditions. The result is shown in Fig. 2.15.

In order to estimate the SiH_3 generation rate in the plasma space, we have also measured the spatial distribution of the $SiH(A^2\Delta)$ emission intensity. This excited radical is produced directly through electron impact on SiH_4 and is lost rapidly by radiative transition nearly at the same place where it is produced. Thus the spatial distribution of the SiH emission intensity represents the distribution of its production rate and thus gives an estimate of the distribution of the SiH_3 production rate.

Under the present experimental conditions, the dominant generation processes of the SiH_3 radicals are

$$SiH_4 + e \rightarrow SiH_3 + H + e, \qquad (2.9)$$
$$SiH_4 + H \rightarrow SiH_3 + H_2, \qquad (2.10)$$

while the dominant loss process is the diffusion. Thus the steady-state spatial distribution of the SiH_3 radical density N satisfies the equation

$$D(d^2N/dx^2) + g(x) = 0, \qquad (2.11)$$

where D is the diffusion constant and g(x) is the generation rate of the radical. We have assumed that, apart from a constant factor, g(x) is equal to the measured SiH emission intensity; this also implies the assumption that the hydrogen atom resulting from reaction (2.9) performs reaction (2.10) nearly in the same spatial position. Integrating Eq. (2.11) with appropriate boundary conditions, we obtain the spatial distribution of the SiH_3 radical.

An example of the calculated spatial distribution of SiH_3 is shown in Fig. 2.16, in which the result is compared with the measured distribution (already shown in Fig. 2.13). Similar analyses were carried out for various H_2 partial pressures in order to estimate the SiH_3 density at x=0 mm. In Fig. 2.17, the growth rate of the a-Si:H film (shown in Fig. 2.15) is plotted against the SiH_3 density at x=0 mm. The figure clearly

shows a linear relationship between the two quantities. Furthermore, the SiH_3 density at x=0 mm is sufficient to explain the growth rate of the film under relatively low H_2 pressure conditions. These observations indicate that the SiH_3 radical plays a major role in the a-Si:H film growth. However, it should be noted that the straight line in Fig. 2.17 does not pass through the origin; the SiH_3 contribution appears to be less important at higher H_2 partial pressures. This off-set is probably ascribed to the contribution of $Si_nH_m(n \geqq 2)$ to the film growth. A detailed discussion on this point is given elsewhere.[8]

3 Measurements of Si Atom Density in Silane Plasmas Using Ultraviolet Absorption Spectroscopy

For the quantitative understanding of the mechanism of a-Si:H formation in silane plasmas, it is also necessary to measure the Si atom density. The Si atom densities in silane plasmas have been measured by using laser induced fluorescence[9,10] and uv absorption spectroscopy.[11] However, the experimental conditions of the reported measurements are rather limited. We have carried out the Si atom density measurements for a wider range of conditions.

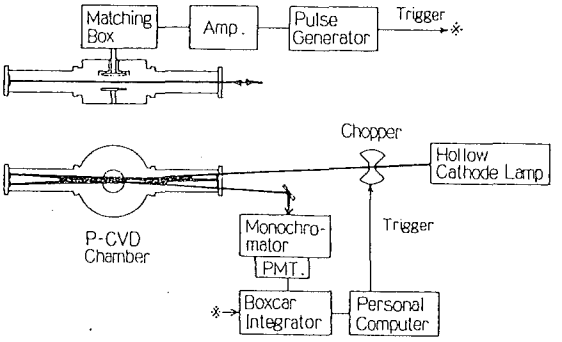

Fig. 3.1. Schematic diagram of the apparatus for uv absorption spectroscopy.

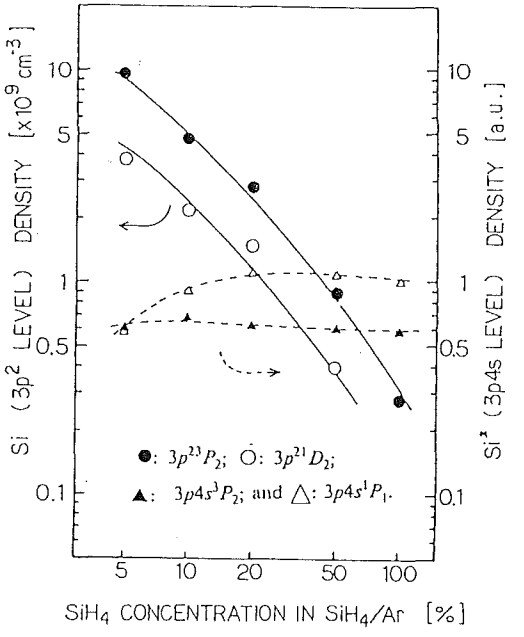

Fig. 3.2. Si atom densities in the RF SiH_4/Ar plasma as a function of the SiH_4 density. The input power is 50 W, the total pressure 50 mTorr, and the total flow rate 10 sccm.

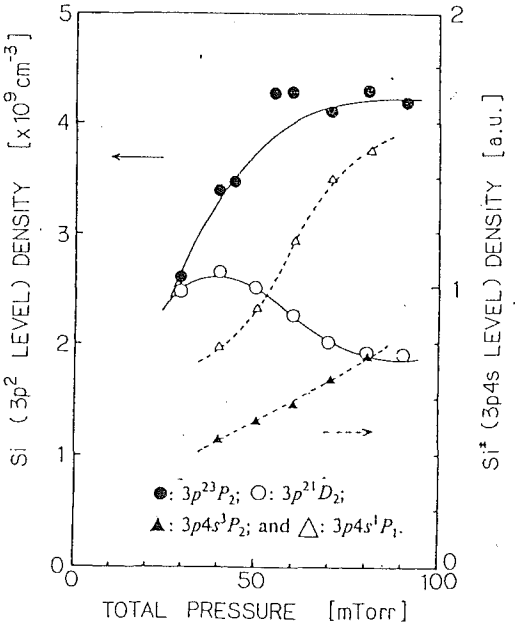

Fig. 3.3. Si atom densities in the RF SiH_4(10%)/Ar plasma as a function of the total pressure. The input power is 50 W and the total flow rate 10 sccm.

3.1 $3p^2\ {}^3P_2$ and $^1D_2$ levels in RF SiH_4/Ar discharge measured using a hollow cathode lamp

Figure 3.1 shows the schematic diagram of the experimental apparatus. A SiH_4/Ar mixture gas was introduced into a plasma CVD chamber equipped with parallel-plate electrodes(10-cm diam. and 3.2-cm apart). The total flow rate was fixed at 10 sccm in all measurements. Modulated RF(13.56 MHz) voltage was applied to the electrodes with RF-on period of 1.2 ms and RF-off period of 0.9 ms. The modulation is used to remove the background disturbance due to the scattering and absorption by dust particles and also to suppress the generation of dust particles. A commercial uv hollow cathode lamp was used as the light source for absorption spectroscopy. The light from the hollow cathode lamp passed through the plasma four times by use of a White-type multiple reflection arrangement so that the total absorption path length was 40 cm.

In order to obtain an absorption signal free from the influence of the plasma emission and other background photons, the transient absorption wave form of the Si atoms was obtained as the difference of the following two signals: (1) the light from the hollow cathode lamp including the plasma emission and other background photons and (2) background photons without the light from the hollow cathode lamp. To improve S/N of the absorption signal, it was averaged by using a boxcar integrator and a personal computer. From the transient waveform thus obtained we can determine the transit intensity (I) in the RF-on period and the transit intensity (I_0) in the RF-off period. We can then calculate the Si atom density from I/I_0.[1)]

Absorption measurements were carried out for the Si atom in the $^3P_2$ and $^1D_2$ levels in the $3p^2$ ground electronic configuration using, respectively, the 251.6- and 288.2-nm absorption lines (whose upper states are 3p4s $^3P_2$ and $^1P_1$, respectively). To convert the absorption intensity into the number density of the Si levels, we assumed a Gaussian line profile at a translational temperature of 400K both for the Si absorption line in the RF plasma and for the emission line in the hollow cathode lamp; the estimate of the temperature is based on the measured rotational temperature for SiH_3 in an RF silane plasma (see Sec. 2). In addition to the absorption measurements, the emission from the excited Si levels (3p4s $^3P_2$ and $^1P_1$) was also measured to obtain the relative values of their densities.

The pressure dependences of the ground and excited Si atom densities are shown in Figs. 3.2 and 3.3. As is seen, the $^1D_2/^3P_2$ density ratio is much higher than the value of 10^{-11} estimated by assuming a thermal equilibrium.[11)] The Si atom densities both in the ground and excited levels were found to increase linearly with increasing RF power. This suggests that they are mainly generated by a single-electron impact on SiH_4, since we expect that the electron temperature does not change much when RF power is varied. On the other hand, the major removal processes will be the diffusion and the reaction with SiH_4 for the $3p^2$ ground levels and will be the radiative decay for the 3p4s excited levels. Therefore, the steady-state densities of the ground and excited levels [N(Si) and N(Si*), respectively] are obtained from the balance equations for the generation and removal processes as

$$N(Si) = k_d(Si) n_e N(SiH_4) / [k_r N(SiH_4) + 1/\tau] \quad (3.1)$$

$$N(Si^*) = k_d(Si^*) n_e N(SiH_4) / A, \quad (3.2)$$

where $N(SiH_4)$ is the SiH_4 density, n_e the electron density, $k_d(X)$ the generation rate of the species X by electron impact, k_r the removal rate con-

stant of Si by reaction with SiH_4, τ the diffusion lifetime, and A the Einstein A coefficient.

In Fig. 3.2, N(Si*) does not change much when SiH_4 partial pressure is varied in SiH_4/Ar. This suggests that $k_d(Si^*)n_eN(SiH_4)$ in Eq. (3.2) is almost constant. Thus we expect that $k_d(Si)n_eN(SiH_4)$ in Eq. (3.1) is also roughly constant. Since $1/\tau$ will not change much, the decrease of N(Si) in Eq. (3.1) should mainly be due to the increase of $k_rN(SiH_4)$. In Fig. 3.2, the fact that N(Si) is inversely proportional to $N(SiH_4)$ suggests that $1/\tau$ is rather less important than $k_rN(SiH_4)$ in Eq. 3.1, i.e., the main removal process of the ground-state Si atoms is the reaction with SiH_4.

In Fig. 3.3, N(Si*) increases with the total pressure. This suggests that $k_d(Si^*)n_eN(SiH_4)$ in Eq. (3.2) and $k_d(Si)n_eN(SiH_4)$ in Eq. (3.1) increase with the total pressure. In Eq. (3.1), the term $k_rN(SiH_4)$ increases linearly with the total pressure. Therefore, the increase of N(Si) will be slower than that of N(Si*), as shown in Fig. 3.3. We notice that the behavior of N(Si) in the $3p^2\ ^3P_2$ level is different from that in $3p^2\ ^1D_2$. This may be understood by considering collisional relaxation processes from $^1D_2$ to $^3P_2$ caused by some particles other than SiH_4.

3.2 $3p^2\ ^1D_2$ level density and translational temperature in RF SiH_4/Ar discharge measured using a ring dye laser

In order to obtain atom densities from the absorption measurement by use of a hollow cathode lamp, we require the knowledge of the emission and absorption line profiles. In the measurements described in Sec. 3.1, we used an assumption that both

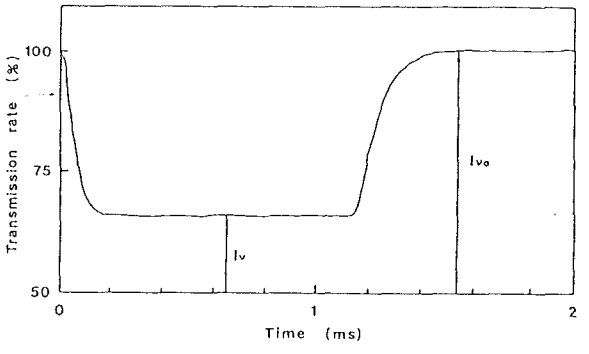

Fig. 3.4. Transient absorption waveform of the 288.2-nm line at the SiH_4(10%)/Ar total pressure of 50 mTorr, the input power of 50 W, and the total flow rate of 10 sccm.

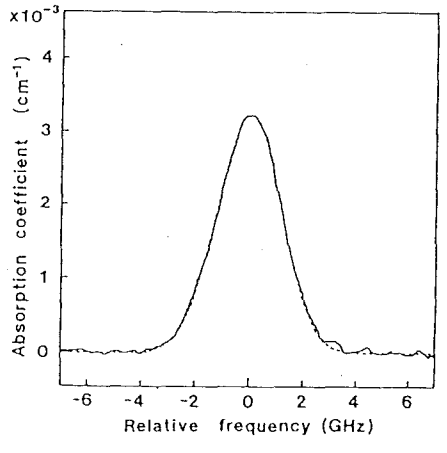

Fig. 3.5. Absorption line profile of the 288.2-nm line. The SiH_4(10%)/Ar total pressure is 50 mTorr, the input power 50 W, and the total flow rate 10 sccm. The broken curve is the calculated Doppler profile at the temperature of 380 K.

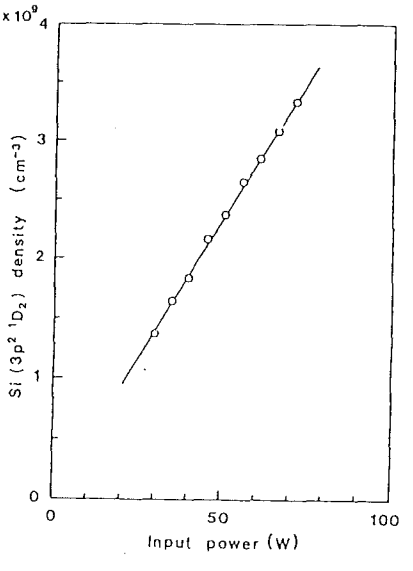

Fig. 3.6. Si atom density as a function of the input power. SiH_4(10%)/Ar total pressure is 50 mTorr and the total flow rate 10 sccm.

line profiles were Gaussian at a translational temperature of 400 K; this may possibly lead to a noticeable error. We have therefore carried out measurements for the Si $3p^2\ ^1D_2$ level by using a ring dye laser as a light source. Since the line width of the laser is much smaller than the line width of the absorption line, we can directly measure the latter by scanning the laser frequency; thus we can expect a higher accuracy of the Si densities derived.

The experimental arrangement is essentially the same as described in Sec. 3.1 except that the hollow cathode lamp is replaced by a ring dye laser (Coherent CR-699-21) pumped by an argon ion laser (Coherent Innova 90-5). The ring dye laser was equipped with an intracavity frequency doubler and provided UV radiation with a linewidth of 1 MHz. The UV output of the laser was tuned to the Si 288.2-nm transition. The laser frequency scan width of 60 GHz was divided into 2048 steps and the absorption profile of the 288.2-nm line was determined by measuring the transmission rate at each frequency. The laser beam passed 12 times through the plasma by use of the White-type multi-reflection system.

Figure 3.4 shows an example of the transient transmission waveform near the 288.2-nm line center for an on-off modulated SiH_4(10%)/Ar plasma. Figure 3.5 shows the measured absorption line profile of the 288.2-nm transition, which is compared with a calculated Gaussian profile reproducing the experimental data most closely. The Si translational temperature derived from the absorption line profile was 380± 20 K and was almost constant in the investigated power range of 30-75 W. Using the measured value of the translational temperature, we can derive the Si atom density (see Sec. 2.1). Figure 3.6 shows the obtained Si atom density as a function of the input power; the result is consistent with the measurement by use of a hollow cathode lamp.

Measurements of the Si($3p^2\ ^1D_2$) atom density and translational temperature by use of the ring dye laser were carried out also for a cw RF SiH_4/Ar plasma. The results were consistent with those for the on-off modulated RF plasma. The translational temperature (~ 400 K) was found to be insensitive to the RF input power (20-35 W) and to the SiH_4(10%)/Ar total pressure (20-45 mTorr).

4 Infrared Laser Spectroscopy of SiH_2 Radical

To study the properties of radicals, high resolution spectroscopic data are indispensable. In contrast to the cases of SiH and SiH_3, the SiH_2 radical has not been studied with high resolution infrared spectroscopy. Here we describe the observation and analysis of the ν_2 (bending) band of SiH_2 in its ground electronic state.

The IRLAS system is described in Sec. 2.1. The absorption cell employed is shown in Fig. 4.1. Phenylsilane ($C_6H_5SiH_3$) was introduced into the cell at very slow flow rate (0.5 sccm at about 1 mTorr) together with a large excess of hydrogen (500 sccm at about 1 Torr). The SiH_2 radical was produced by the ArF excimer laser (193 nm) photolysis of phenylsilane. The ArF laser was pulsed at 20 Hz with energies of 70-80 mJ/pulse. Figure. 4.2 shows the transient absorption profile of the band of SiH_2. The decay of the absorption signal is well reproduced by a single-exponential curve with a time constant of 14 μ s; the decay time constant varied with the hydrogen pressure. The absorption signal was recorded for three different gate settings (also shown in Fig. 4.2) while scanning the diode laser wavelength slowly. Using the difference of the intensities of the three records, we could distinguish the SiH_2 signal from

other species showing different temporal behavior. About 50 lines were observed in the region of 920-1090 cm^{-1}; they are shown in Table 4.1.

Assignment of the observed spectrum, though patchy because of the diode laser's mode gaps, was carried out by comparison with a simulated spectrum, which was derived with the rotational constants for the ground state from Dubois' optical data[12-14] and vibration-rotation constants taken from a similar molecule H_2S. The Hamiltonian used for the

Table 4.1 Observed transitions of the SiH_2 ν_2 band (cm^{-1})

Transition								Transition							
J'	Ka'	Kc'	J"	Ka"	Kc"	Obs	Obs-Calc	J'	Ka'	Kc'	J"	Ka"	Kc"	Obs	Obs-Calc
7	0	7	8	1	8	934.28713	0.00009	4	3	2	4	2	3	1021.49980	-0.00009
7	1	7	8	0	8	834.28713	0.00009	5	2	3	5	1	4	1027.58093	0.00022
6	0	6	7	1	7	942.18567	-0.00030	2	2	1	1	1	0	1027.75163	-0.00043
6	1	6	7	0	7	942.18567	-0.00042	5	1	4	5	0	5	1034.46680	0.00006
3	2	1	4	3	2	948.25676	-0.00031	5	0	5	4	1	4	1038.97494	-0.00014
4	2	3	5	1	4	951.90420	-0.00054	8	5	4	8	4	5	1041.19186	-0.00002
6	1	6	6	2	5	956.01473	0.00051	4	2	3	3	1	2	1045.73931	0.00026
4	0	4	5	1	5	957.67440	0.00082	3	3	1	2	2	0	1045.73931	0.00023
4	1	4	5	0	5	957.68082	0.00083	6	0	6	5	1	5	1045.93585	0.00022
3	1	2	4	2	3	958.05119	-0.00043	6	1	6	5	0	5	1045.93585	-0.00046
3	0	3	4	1	4	965.24094	0.00002	5	1	4	4	2	3	1048.63867	-0.00006
3	1	3	4	0	4	965.28781	-0.00003	5	2	4	4	1	3	1048.91647	-0.00018
7	2	5	7	3	4	969.98631	0.00009	3	3	0	2	2	1	1049.76028	0.00025
2	1	2	3	0	3	972.89771	-0.00016	7	0	7	6	1	6	1052.77709	0.00017
6	3	4	6	4	3	975.90860	-0.00032	7	1	7	6	0	6	1052.77709	0.00008
5	4	1	5	5	0	988.11181	0.00005	6	1	5	5	2	4	1056.17753	0.00050
2	0	2	2	1	1	988.57129	0.00044	6	2	5	5	1	4	1056.22309	-0.00070
5	3	2	5	4	1	991.93892	0.00070	8	0	8	7	1	7	1059.49961	-0.00023
3	2	1	3	3	0	992.39681	-0.00026	8	1	8	7	0	7	1059.49961	-0.00025
1	0	1	1	1	0	994.29833	-0.00019	7	1	6	6	2	5	1063.51040	0.00006
1	1	0	1	0	1	1003.41630	-0.00017	4	4	1	3	3	0	1064.29917	0.00026
3	2	1	3	1	2	1009.89358	0.00030	8	2	7	7	1	6	1070.71452	0.00008
4	3	1	4	2	2	1011.32543	-0.00014	5	5	0	4	4	1	1084.36731	0.00005
2	2	1	2	1	2	1012.94253	-0.00019	10	2	9	9	1	8	1084.76765	0.00000
6	5	1	6	4	2	1018.97953	0.00022	10	1	9	9	2	8	1084.76765	0.00003
6	4	2	6	3	3	1019.14163	-0.00040	12	0	12	11	1	11	1085.19874	0.00002
5	5	0	5	4	1	1020.89212	-0.00029	12	1	12	11	0	11	1085.19874	0.00002

Table 4.2 Molecular constants of SiH_2 ν_2 band (in cm^{-1})

Const	v=0	v_2=1	Const	v=0	v_2=1
A	8.09866(14)	8.36906(14)	Φ_J	0.28×10^{-6}(fixed)	0.39×10^{-6}(fixed)
B	7.023966(94)	7.150716(86)	Φ_{JK}	-0.155×10^{-5}(fixed)	-0.194×10^{-5}(fixed)
C	3.702685(35)	3.646352(30)	Φ_{KJ}	$-0.15(25)\times10^{-6}$	$0.62(25)\times10^{-6}$
Δ_J	$0.4610(11)\times10^{-3}$	$0.5199(12)\times10^{-3}$	Φ_K	0.135×10^{-5}(fixed)	0.261×10^{-5}(fixed)
Δ_{JK}	$-0.14219(46)\times10^{-2}$	$-0.16953(77)\times10^{-2}$	ϕ_J	0.14×10^{-6}(fixed)	0.19×10^{-6}(fixed)
Δ_K	$0.2340(13)\times10^{-2}$	$0.29236(62)\times10^{-2}$	ϕ_{JK}	-0.48×10^{-6}(fixed)	-0.62×10^{-6}(fixed)
δ_J	$0.20521(55)\times10^{-3}$	$0.23438(60)\times10^{-3}$	ϕ_K	$-0.36(38)\times10^{-6}$	$0.20(23)\times10^{-5}$
δ_K	$-0.670(56)\times10^{-4}$	$0.382(57)\times10^{-4}$	ν_0		998.62413(29)

analysis is[15]

$$H_{vr} = E_v + (B+C)J^2/2 + [A-(B+C)/2]J_a^2 + (B-C)(J_+^2+J_-^2)/4 - \Delta_J J^4 - \Delta_{JK} J_a^2 J^2 - \Delta_K J_a^4 - \delta_J J^2 (J_+^2+J_-^2) - \delta_K [J_a^2, J_+^2+J_-^2]_+/2 + \Phi_J J^6 + \Phi_{JK} J^4 J_a^2 + \Phi_{KJ} J^2 J_a^4 + \Phi_K J_a^6 + \phi_J J^4 (J_+^2+J_-^2) + (\phi_{JK}/2) J^2 [J_a^2, J_+^2+J_-^2]_+ + \phi_K [J_a^4, J_+^2+J_-^2]_+/2, \quad (4.1)$$

where $[A,B]_+=AB+BA$ and $J_\pm=J_b \pm iJ_c$. In table 4.2 the molecular constants derived in this study are listed; the accuracy of the results has been much improved over that obtained from optical spectra.

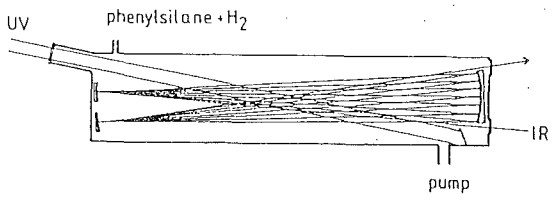

Fig. 4.1. Absorption cell.

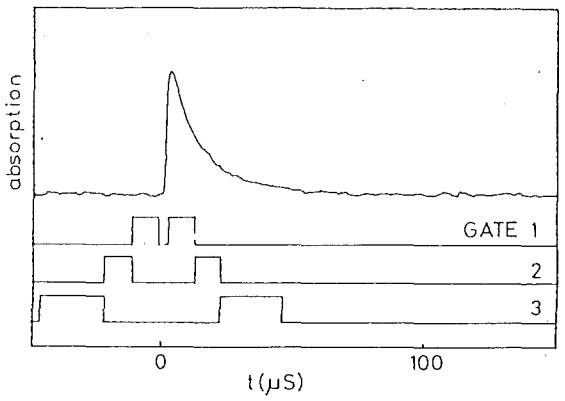

Fig. 4.2. Time profile of an absorption line in the SiH_2 ν_2 band. Three pairs of gates shown below the signal were employed to observe time resolved spectra.

5 Measurements of Radical Densities in Fluorocarbon Plasmas Using Infrared Diode Laser Absorption Spectroscopy

Fluorocarbon plasmas are used for dry etching of semiconductor materials. In order to clarify etching mechanisms quantitatively, we need information about radical densities in the plasma. We have successfully applied the IRLAS method to determine the CF and CF_3 radical densities in some fluorocarbon plasmas.

5.1 CF density in DC pulsed CF_4/H_2 discharge

The IRLAS system and the discharge tube employed were the same as described in Sec. 2.1. The CF_4/H_2 gas mixture was excited by DC pulsed voltage with the repetition frequency of 9 Hz, the pulse width of 1.1 ms and the peak current of 1 A. The absorption band of the CF radical in the ground electronic states, $X^2\Pi_{1/2}$ and $X^2\Pi_{3/2}$ ($v:1\leftarrow 0$), appears in the 1200-1300 cm^{-1} region. Each rovibrational line was identified using N_2O as a reference gas.

Figure 5.1(a) shows the absorption profile of the $R_1(4.5)$ and $R_2(4.5)$ lines measured at the peak of the transient absorption waveform. The R_1 line is split into two components because of Λ-type doubling, whereas the splitting of $R_2(4.5)$ is too small to be observed. Figure 5.1(b) shows the transient absorption waveform measured at pressures of CF_4/H_2=42/258 mTorr and the total flow rate of 105 sccm. In this condition, the CF radical densities in 8 rotational states were determined to obtain the rotational and spin temperatures. We found that the rotational and spin temperatures were equal:

$$T_r = T_s = 320 \pm 20 \text{ K}.$$

The total density of $CF(X^2\Pi)$ in the ground vibrational state was then

calculated using the partition function, resulting in

$$N(X^2\Pi) = (1.33 \pm 0.06) \times 10^{12}\ cm^{-3};$$

the required Einstein A coefficient was taken from an ab-initio calculations.[16]

The dependence of the CF radical density on the total pressure and the H_2 partial pressure was investigated. The results are shown in Fig. 5.2 (a) and (b). As we see below, the loss rate of CF decreases with increasing pressure. Therefore, the results in Fig. 5.2 suggest that the generation rate of CF should decrease with increasing pressure presumably because the electron temperature decreases with increasing pressure.

The transient absorption intensity of the $R_2(4.5)$ line was measured at various pressures and its decay part after the turn off of the discharge was analyzed. All of the decay curves were well fitted to a single-exponential function. The dependence of the decay lifetime τ on the H_2 partial

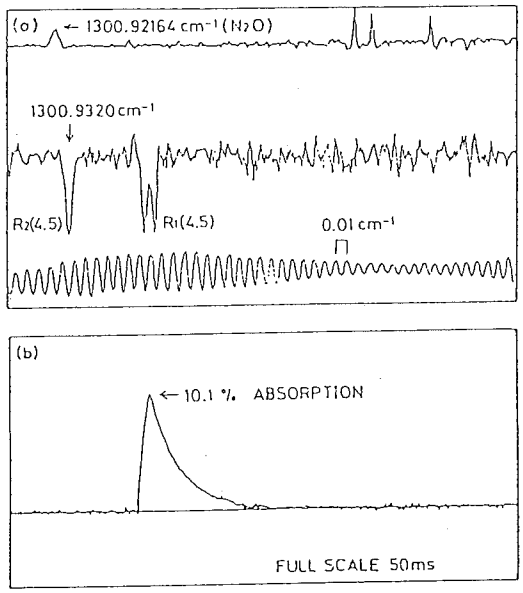

Fig. 5.1. (a) Absorption profile of the CF lines (the middle trace). (b) Transient absorption waveform of the $R_2(4.5)$ line.

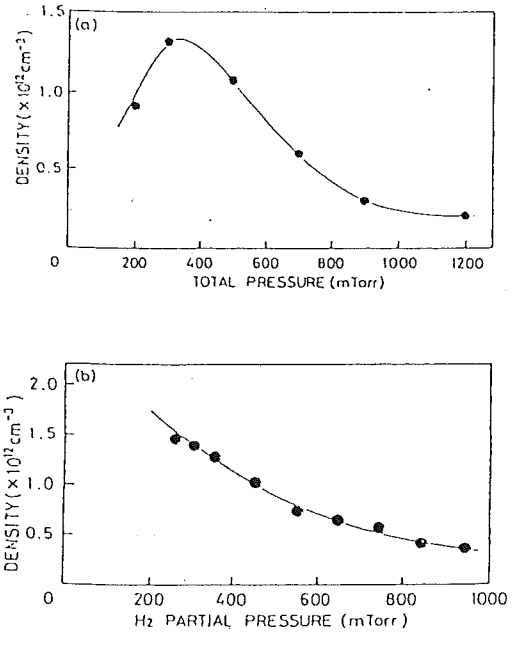

Fig. 5.2. (a)CF radical density as a function of the $CF_4(14\%)/H_2$ total pressure. (b)CF radical density as a function of the H_2 partial pressure at the CF_4 partial pressure of 42 mTorr.

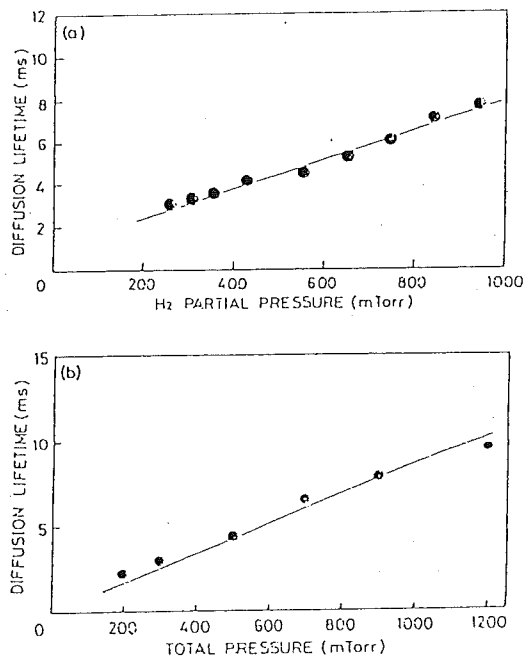

Fig. 5.3. Diffusion lifetime of the CF radical (a) as a function of the H_2 partial pressure at the CF_4 pressure of 42 mTorr and the flow rate of 15 sccm, and (b) as a function of the $CF_4(14\%)/H_2$ total pressure.

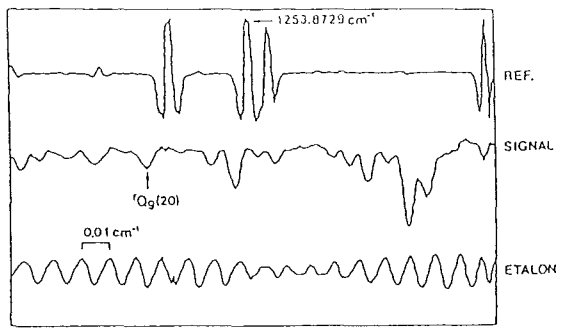

Fig. 5.4. Absorption line profile of the CF_3 $^rQ_9(20)$ line.

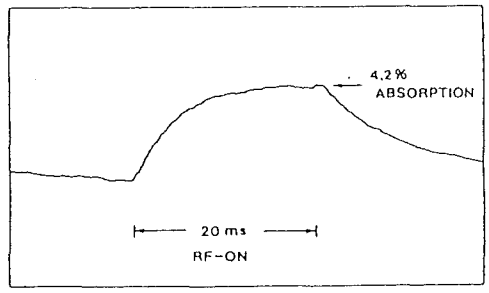

Fig. 5.5. Transient absorption waveform of the CF_3 $^rQ_9(20)$ line at the CHF_3 pressure of 50 mTorr, the flow rate of 90 sccm, and the RF power of 145W.

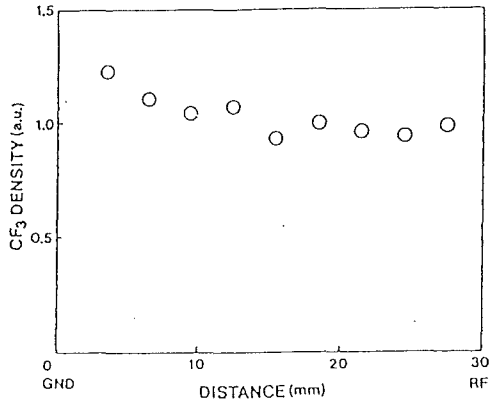

Fig. 5.6. Spatial distribution of the CF_3 radical density at the CHF_3 pressure of 50 mTorr, the flow rate of 90 sccm, and the RF power of 145W.

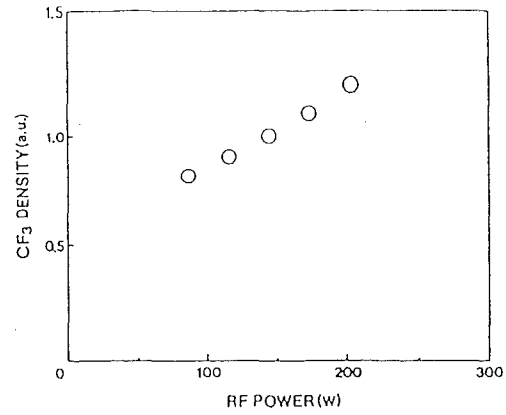

Fig. 5.7. Power dependence of the CF_3 radical density at the CHF_3 pressure of 50 mTorr and the flow rate of 90 sccm.

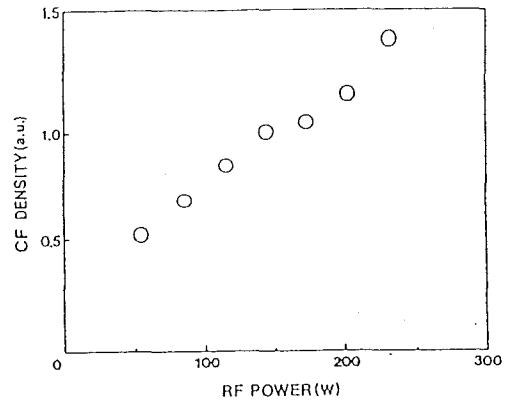

Fig. 5.8. Power dependence of the CF radical density at the CHF_3 pressure of 50 mTorr and the flow rate of 90 sccm.

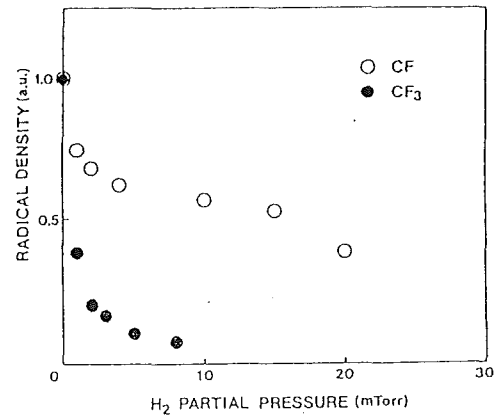

Fig. 5.9 H_2 partial pressure dependence of the CF_3 and CF radical densities. The CHF_3 pressure was 50 mTorr, its flow rate 90 sccm, and the RF power 145W.

pressure and on the total pressure is shown in Fig. 5.3. As seen in the figure, τ increases linearly with increasing pressure. This indicates that the diffusion is the dominant loss process of the CF radical. Using the results in Fig. 5.3 and Blanc's low (see Sec. 2.1), the diffusion coefficients of CF in H_2 and CF_4 are estimated to be

$$D(CF \text{ in } H_2)=630\pm 30 \text{ cm}^2\cdot\text{Torr}\cdot\text{s}^{-1}$$
$$D(CF \text{ in } CF_4)=230\pm 10 \text{ cm}^2\cdot\text{Torr}\cdot\text{s}^{-1}.$$

5.2 CF_3 and CF densities in RF CHF_3 discharge

The experimental arrangement was essentially the same as described in Sec. 2.3. The on-off modulated RF(13.56 MHz) voltage was applied to the parallel-plate electrodes with on-period of 20 ms and off-period of 38 ms. The input power in RF on-period was typically 145 W. The CHF_3 pressure was fixed at 50 mTorr and the flow rate at 90 sccm. The infrared laser beam was located at 18.5 mm above the lower (grounded) electrode, except for measuring the spatial distribution of the radical density.

The absorption band ($\nu_3 : 1 \leftarrow 0$) of the CF_3 radical in the electronic ground state (X^2A_1) appears in the 1230-1270 cm^{-1} region and was identified with the aid of the N_2O reference spectrum. Figures 5.4 and 5.5 show, respectively, the absorption line profile and transient absorption waveform of the $^rQ_9(20)$ line, which was used to determine the CF_3 radical density.

The CF radical densities in 9 rotational levels were measured to obtain the rotational temperature. The value of

$$Tr = 350\pm 40 \text{ K}$$

thus determined was used to calculate both the CF and CF_3 densities.

Figure 5.6 shows the spatial distribution of the CF_3 radical density. It is nearly constant between the electrodes. This fact, together with the relatively long lifetime ($\sim$ 15 ms, see Fig. 5.5) of CF_3, indicates that the sticking probability of the CF_3 radical to the electrodes is small. Thus, the CF_3 radicals are expected to spread out from the plasma region, which makes it difficult to estimate the absorption path length. Assuming that the CF_3 radicals exist only between the 20-cm diameter electrode plates, we can estimate the upper limit of the CF_3 density, which is 2×10^{14} cm^{-3} at the point of 18.5 mm in Fig. 5.6. A similar estimate for the CF density is 4×10^{12} cm^{-3} under the same condition.

Figures 5.7 and 5.8 show the RF power dependence of the CF_3 and CF radical densities, respectively. In the measured power range, the CF radical density increases more rapidly than the CF_3 density with increasing RF power.

Figure 5.9 shows the H_2 partial pressure dependence of the CF_3 and CF radical densities. Only a small addition of H_2 to CHF_3 reduces the CF_3 and CF densities significantly, and the CF_3 density decreases more rapidly than CF.

6 Method of Determining Radiative Transition Probabilities of Radicals Using Saturated Laser Induced Fluorescence

In the measurement of radical densities by use of spectroscopic techniques, the knowledge of radiative transition probabilities or Einstein A coefficients is essential. A method that is usually employed to deter-

mine transition probabilities involves the measurement of optical emission or absorption intensities for known density of molecules or atoms, or to measure a radiative lifetime and derive transition probabilities with the use of known branching ratios. However, for radicals, emission and absorption methods are not suitable since their densities are usually not known; lifetime methods are also not suitable for radicals with a predissociating upper state since the branching ratio between the radiative and nonradiative decay channels is difficult to determine. Here we propose a new method to determine transition probabilities which utilizes the saturation behavior of a laser induced fluorescence (LIF) signal; this method does not require the knowledge of upper and lower level populations and does not depend on lifetime measurements. To demonstrate that the new method works properly, we have applied the method to a determination of the transition probabilities of some Ar lines and the $R_{12}(1.5)$ line of SiH $A^2\Delta - X^2\Pi$, 0-0 band transitions.

Principle of the method

Consider a non-degenerate two-level system irradiated by a pulsed laser radiation tuned to the resonance frequency of the system. If the laser pulse width is much shorter than the radiative and collisional relaxation times of the levels (the spontaneous emission during laser irradiation can thus be neglected), a rate equation analysis predicts that the upper-level density (N_u) just after the laser irradiation is given by

$$N_u=(N_0/2)[1-\exp(-2B\rho\,\tau)], \qquad (6.1)$$

where N_0 is the lower-level density before laser irradiation, B the Einstein B coefficient, and ρ and τ the energy density and the width of the laser pulse, respectively. The LIF signal intensity I_F is proportional to the upper-level density and is given by

$$I_F=C[1-\exp(-2B\rho\,\tau)], \qquad (6.2)$$

where C is a proportionality constant. Equation (6.2) indicates that I_F as a function of ρ saturates when ρ becomes $> 1/B\tau$. Therefore, we can determine the B value by measuring I_F as a function of ρ and by fitting the theoretical saturation curve (6.2) to the measured values. Since the Einstein B coefficient is proportional to the spontaneous transition probability, we can then determine the transition probability.

In the actual experimental procedure, we measure LIF saturation curves for a pair of spectral lines; one of the spectral line is used as a reference and its transition probability should be known. In this case we need to measure ρ only on an arbitrary scale. A curve fitting analysis of the two saturation curves gives the two transition probabilities on an arbitrary scale. Since we know the absolute value of one of the transition probabilities, we can readily obtain the absolute value of the other. In the actual data analysis, we have taken into account the effects of the following facts: the angular-momentum degeneracy in the upper and lower levels, the excitation anisotropy, and the spatial distribution of the laser field intensity.[17)]

Experimental setup

The block diagram of the experimental arrangement is shown in Fig. 6.1. Measurements were made for a 13.56-MHz RF plasma in Ar or Ar/SiH4 mixture. The same plasma reactor as described in Sec. 3 was used. The total pressure and RF power were maintained at 50 mTorr and 10 W respectively. At this pressure and RF power, any collisional effects caused by the parent gas and electrons should be negligible. The laser

system consisted of a dye laser (Quanta Ray PDL-2) pumped by a pulsed Nd:YAG laser (Quanta Ray DCR-3) and a wavelength extender (Quanta Ray WEX-1). The laser system, operated at 10-Hz repetition frequency, produced linearly polarized 0.5-mJ 5-ns light pulses at around 420 nm, which were strong enough to attain the saturation of the LIF intensity. The laser beam was adjusted to pass through the plasma in parallel with the electrode plates. The LIF signal was collected by a lens of 150-mm focal length at right angle with the laser beam, was selected by a 200-mm monochromator, and was detected by a photomultiplier. The output signal of the photomultiplier was recorded by a digitizing oscilloscope (HP HP4111D) and was averaged by a personal computer.

Results and discussion

In order to demonstrate that the proposed method yielded reliable results, we first measured the relative transition probabilities of four Ar I lines (419.8, 415.9, 427.2, and 426.6 nm) with the 415.9-nm line used as a reference line. The transition probabilities of these lines were measured previously with relatively high precision.[18] An example of the LIF saturation curves for the 415.9- and 426.6-nm lines is shown in Fig. 6.2. From such a pair of curves, we derived the relative transition probabilities of the two lines. The final results for the four Ar lines are shown in Table 6.1. The measured values agree with the values reported previously.[18)-20)]

Next, the method was applied to the determination of the transition probability of the $R_{12}(1.5)$ line of the SiH $A^2\Delta - X^2\Pi$, 0-0 band transitions, with the Ar 415.9-nm transition used as a reference line. The $R_{12}(1.5)$ line was selected since it does not overlap other SiH excitation lines and can produce a strong LIF intensity. The measured LIF saturation curves are shown in Fig. 6.3, from which the ratio of the transition probabilities of the SiH and Ar lines is derived as

$$A_{SiH}/A_{Ar}=0.50\pm 0.13.$$

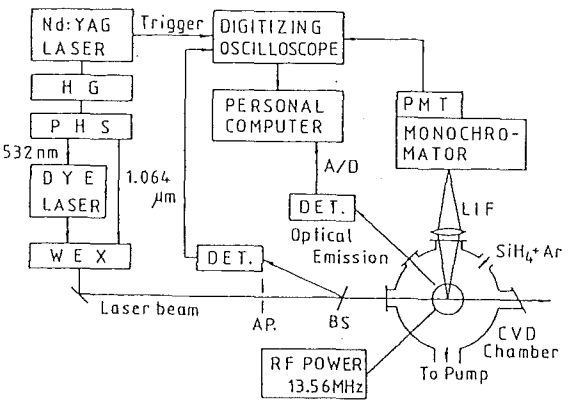

Fig. 6.1. Block diagram of the experimental arrangement

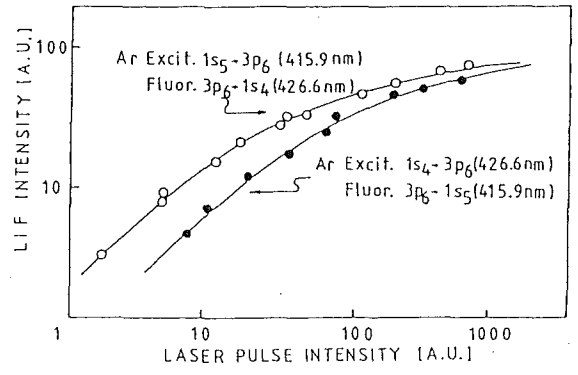

Fig. 6.2. Saturation behavior of the LIF intensities of Ar lines.

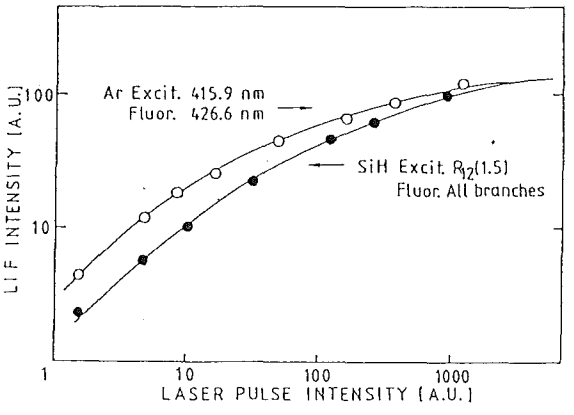

Fig. 6.3. Saturation behavior of the LIF intensity of a SiH line compared with that of an Ar line.

Using the transition probability of the Ar 415.9-nm line reported in Ref. 18, the A value of the SiH line is estimated to be

$$A_{SiH}=(0.75\pm 0.20)\times 10^{6}\ s^{-1}.$$

On the other hand, the transition probability of the SiH line obtained by combining the radiative lifetime and the branching ratio is given by

$$A(SiH)=(1/\tau)\cdot q(0,0)\cdot S/(2J+1)$$

where τ is the radiative lifetime, q(0,0) the Franck-Condon factor of the 0-0 band, S the Honl-London factor, and J the rotational quantum number of the upper level. By using measured value of τ ,[21] theoretical q(0,0),[22] and S calculated from general formulas[23] with parameters derived from analyses of observed spectra,[24] A(SiH) is derived to be $0.88\times 10^{6}\ s^{-1}$. Our result agrees with this value within the experimental uncertainty.

From the indicated results, we may conclude that the proposed method can actually be used to determine unknown transition probabilities. As seen in Table 6.1, the estimated uncertainties of the relative transition probabilities obtained are around 30%. Though this level of accuracy is not very high, the present method could well be useful in cases where difficulty exists in applying conventional methods for determining transition probabilities, e.g., in measurements for a radical with a predissociating upper state. The estimated uncertainties of the results in Table 6.1 mainly results from statistical errors; the scatter of the data probably comes from the fluctuations of the plasma and the laser pulse intensity. Reduction of these fluctuations, as well as measuring the LIF saturation behavior for higher laser intensities, would improve the accuracy of the results.

Table 6.1. Relative transition probabilities of Ar and SiH lines
The value for Ar 415.9-nm line is normalized to 1.

Transition	Wavelength (nm)	Relative transition probabilities This work	Jones[a]	Lilly[b]	Buese[c]
Ar I					
$3p_5$-$1s_4$	419.8	1.21± 0.39	1.65	1.21	1.78
$3p_6$-$1s_5$	415.9	1.00	1.00	1.00	1.00
$3p_7$-$1s_4$	427.7	0.63± 0.23	0.52	0.87	0.60
$3p_6$-$1s_4$	426.6	0.23± 0.06	0.20	0.22	0.25
SiH					
$R_{12}(1.5)$	414.6	0.50± 0.13	0.59[d]	0.52[d]	0.63[d]

[a]Ref.18 [b]Ref.19 [c]Ref.20 d:assuming $A(SiH)=0.88\times10^{6}\ s^{-1}$

7 Conclusion

A method of measuring radical densities in processing plasmas has been established by using infrared diode laser absorption spectroscopy. The densities of the SiH_3 and SiH radicals in silane plasmas were measured under various discharge conditions. From the study of the correlation between the SiH_3 density and the a-Si:H film growth rate, it was demonstrated that the SiH_3 radical is the most important precursor for the film formation. The diffusion coefficients of SiH_3 in SiH_4 and H_2 and some reaction rate constants for SiH_3 and SiH were also determined.

A high resolution infrared spectrum of the SiH_2 radical was studied by using IRLAS to obtain molecular constants with high accuracy.

In addition to molecular radicals, the Si atom densities in silane plasmas were studied by using uv absorption spectroscopy; both a hollow cathode lamp and a ring dye laser were used as a light source. The densities of the $^1D_2$ and $^3P_2$ levels (ground electronic configuration) and the translational temperature of the $^1D_2$ level were determined under various discharge conditions.

An IRLAS study was also carried out for fluorocarbon plasmas (pulsed DC CF_4 and RF CHF_3 discharges). The CF and CF_3 radical densities in these plasmas were determined under various discharge conditions. The diffusion coefficients of CF in CF_4 and H_2 were determined.

We have also developed a new method of determining radiative transition probabilities; the method only relies on the saturation behavior of the LIF intensity and therefore is suitable for radicals with a predissociating upper state.

References

1)A.C.G. Mitchel and M.W. Zemansky, *Resonance Radiation and Excited Atoms* (Cambridge Univ. Press, London 1971),chap.3

2)W.D. Allen and H.F. Schaefer III, Chem. Phys. 108(1986)243

3)W. Gordy and R.L. Cook, *Microwave Molecular Spectra*(Interscience Publisher, New York, 1970),chap. 3

4)E.W. McDaniel, *Collision Phenomena in Ionized Gases*(John Wiley & Sons, Inc., New York, 1964)pp455-457

5)J.P.M. Schmitt, P. Gressier, M. Krishnan, G. de Rosney and J. Perrin, Chem. Phys. 84(1984)281

6)A. Matsuda, K. Nomoto, Y. Takeuchi, A. Suzuki, A. Yuuki and J. Perrin, Surf. Sci. 227(1990)50

7)N. Itabashi, N. Nishiwaki, M. Magane, S. Naito, T. Goto, A. Matsuda, C. Yamada and E. Hirota, Jpn. J. Appl. Phys. 29(1990)L505

8)N. Itabashi, M. Magane, S. Naito, T. Goto, A. Matsuda, C. Yamada and E. Hirota, to be published in Jpn. J. Appl. Phys. (1992)

9)R.M. Roth, K.G. Spears and G. Wong, Appl. Phys. Lett. 45(1984)28

10)Y. Takubo, Y. Takasugi, M. Yamamoto, J. Appl. Phys. 64(1988)1050

11)K. Tachibana, H. Tadokoro, H. Harima and Y. Urano, J. Phys. D 15(1982)177

12)I. Dubois, Can. J. Phys. 46(1968)2485

13)I. Dubois, G. Duxbury and R.N. Dixon, J. Chem. Soc. Farady Trans. II 71(1975)799

14)I. Duois, G. Herzberg and R.D. Verma, J. Chem. Phys. 47(1967)4262

15)J.K.G. Watson, *Vibrational Spectra and Structure*, vol.6(Elsevier, Amsterdam 1977), ed. J.R. During

16)B.A. Hess and R.J. Buenker, Chem. Phys. 101(1986)211

17)K. Okuda, K. Furuto, S. Kishimoto, A. Kono and T. Goto, to be published in J. Quant. Spectrosc. Radiat. Transfer (1992)

18)D. W. Jones and W. L. Wiese, Phys. Rev. A39(1989)110

19)R. A. Lilly, J. Opt. Soc. Am. 66(1976)245

20)J. Bues, T. Haag, and J. Richter, Astron. Astrophys. 2(1969)249

21)W. Bauer, K. H. Becker, R. Duren, C. Hubrich, and R. Meuser, Chem. Phys. Lett. 108(1984)560

22)M. Lewerenz, P. J. Bruna, S. D. Peyeimhoff, and R. J. Buenker, Mol. Phys. 49(1983)1

23)R. F. M. Bennet, Mon. Not. R. Astrn. Soc. 147(1970)35

24)L. Klynning and B. Lindgren, Arkiv. Pysik. 33(1966)73

SUPPORT AND REPORTS

Amount of Grant-in-Aid and main equipments installed by the grant

'88: ¥14,000,000, a YAG laser
'89: ¥15,400,000, a dye laser, an rf power supply, a capacitance manometer, an rf chamber, an IR diode laser
'90: ¥15,000,000, a wavelength extender, an IR diode laser, optical devices for ring dye and IR laser systems

Reports through this research

1)Naoshi ITABASHI, Kozo KATO, Nobuki NISHIWAKI, Toshio GOTO, Chikashi YAMADA and Eizi HIROTA, Measurement of the SiH_3 Radical Density in Silane Plasma Using Infrared Diode Laser Absorption Spectroscopy, Jpn. J. Appl. Phys. vol.27, no.8(1988)L1565

2)Kozo KATO, Naoshi ITABASHI and Toshio GOTO, Measurements of SiH ($X\ ^2\Pi$;v=0) Radicals in Ar/SiH_4 Plasma Using an Infrared Diode Laser, Proc. Jpn. Symp. Plasma Chem. vol.1(1988)11

3)Naoshi ITABASHI, Kozo KATO, Nobuki NISHIWAKI, Toshio GOTO, Chikashi YAMADA and Eizi HIROTA, Diffusion Coefficient and Reaction Rate Constant of the SiH_3 Radical in Silane Plasma, Jpn. J. Appl. Phys. vol.28, no.2(1989)L325

4)後藤俊夫，廣田榮治，レーザー吸収法によるシランプラズマ内の非発光ラジカル計測，レーザー研究 vol.17, no.8(1989)595

5)Chikashi YAMADA, Eizi HIROTA, Nobuki NISHIWAKI, Naoshi ITABASHI, Kozo KATO and Toshio GOTO, Detection of Silylene ν_2 Band by Infrared Diode Laser Kinetic Spectroscopy, J. Chem. Phys. vol.91, no.8(1989)4582

6)Toshio GOTO, Measurement Method of Neutral Non-Emissive Radicals in Processing Plasma, Proc. Jpn. Symp. Plasma Chem. vol.2(1989)23

7)Naoshi ITABASHI, Nobuki NISHIWAKI, Mitsuo MAGANE, Susumu NAITO, Toshio GOTO, Akihisa MATSUDA, Chikashi YAMADA and Eizi HIROTA, Spatial Distribution of SiH_3 Radicals in RF Silane Plasma, Jpn. J. Appl. Phys. vol.29, no.3(1990)L505

8)Naoshi ITABASHI, Nobuki NISHIWAKI, Mitsuo MAGANE, Susumu NAITO, Toshio GOTO, Akihisa MATSUDA, Chikasi YAMADA and Eizi HIROTA, Jpn. J. Appl. Phys. vol.29, no.3(1990)585

9)後藤俊夫，反応性プラズマの新しい診断技術，J. IEE. Jpn. vol.110, no.3(1990)181

10)Mitsuo MAGANE, Naoshi ITABASHI, Nobuki NISHIWAKI, Toshio GOTO, Chikashi YAMADA and Eizi HIROTA, Measurements of the CF Radical in DC Pulsed CF_4/H_2 Discharge Plasma Using Infrared Diode Laser Absorption Spectroscopy, Jpn. J. Appl. Phys. vol.29, no.5(1990)L829

11)後藤俊夫，プラズマＣＶＤ内における非発光ラジカルの計測，化学工業 vol.54, no.9(1990)32

12)Masafumi SAKAKIBARA, Mineo HIRAMATSU and Toshio GOTO, Measurement of Si Atom Density in Radio-Frequency Silane Plasma Using Ultraviolet Absorption Spectroscopy, J. Appl. Phys. vol.69, no.6(1991)3467

13)後藤俊夫，赤外半導体レーザー吸収分光法によるラジカル計測，光学 vol.20, no.1(1991)10

14)Mineo HIRAMATSU, Masafumi SAKAKIBARA, Mitsuteru MUSHIGA and Toshio GOTO, Measurement of the Density and Translational Temperature of Si($3^p2\ ^1D_2$) Atoms in RF Silane Plasma Using UV Laser Absorption Spectroscopy, Meas. Sci. Technol. vol.2, no.7(1991)641

15)Naoshi Itabashi, Mitsuo MAGANE, Susumu NAITO, Toshio GOTO, Akihisa MATSUDA, Chikashi YAMADA and Eizi HIROTA, Correlation Between the SiH_3 Radical Density and the Growth Rate of a-Si:H Thin Film, Jpn. J. Appl. Phys. (1992)(to be published)
16)Kenichi OKUDA, Ken FURUTO, Shigeru KISHIMOTO, Akihiro KONO and Toshio GOTO, Determination of Transition Probabilities Using the Saturation Behavior of Laser Induced Fluorescence, J. Quant. Spectrosc. Radiat. Transfer (1992)(to be published)

(International conferences)
1 report in 41st Gaseous Electronics Conf.(Minneapolis) '88FY
1 report in IEEE Int. Conf. on Plasma Science(Buffalo) '89FY
1 report in 42nd Gaseous Electronics Conf.(Palo Alto) '89FY
1 report in Int. Symp. Laser-Aided Plasma Diagnostics(Fukuoka) '89FY
1 report in IEEE Int. Conf. on Plasma Science(Oakland) '90FY
2 reports in 10th Euro. Sect. Conf. on Atom. and Mol. Phys. of Ionized Gases(Orleans) '90FY
2 reports in Int. Seminar on Reactive Plasmas(Nagoya) '91FY

(Domestic conferences)
3 reports in 1st Jpn. Symp. Plasma Chem. '88FY
1 report in 電気学会プラズマ研究会 '88FY
3 reports in 6th Symp. Plasma Processing '88FY
4 reports in 2nd Jpn. Symp. Plasma Chem. '89FY
4 reports in 7th Symp. Plasma Processing '89FY
1 report in 13th Symp. ISIAT '90FY
2 reports in 3rd Jpn. Symp. Plasma Chem. '90FY
3 reports in 8th Symp. Plasma Processing '90FY
1 report in 4th Jpn. Symp. Plasma Chem. '91FY
3 reports in 9th Symp. Plasma Processing '91FY